Compact Microstrip-Based Folded-Shorted Patches by PCB Technology for Use on Microsatellites

Symon K. Podilchak, *Member, IEEE,* Andrew P. Murdoch, *Member, IEEE,* Yahia M. M. Antar, *Life Fellow, IEEE,*

***Abstract*—A compact printed circuit board (PCB) antenna for use on microsatellite was designed and measured for UHF low data rate communication applications. In particular, the miniaturized and fully integrated antenna structure consists of an array of four, linearly polarized folded-shorted patch elements placed in a sequential rotation with a coupler-based feeding circuit to achieve circular polarization. Dimensions of the fabricated and measured PCB antenna are $0.2\lambda_0$ by $0.2\lambda_0$ by $0.05\lambda_0$. Measured gain values are greater than 0.4 dBic at 398 MHz. A design procedure for the microstrip-based antenna is provided along with a transmission line model that accurately predicts the operation and resonant frequency of the miniaturized patches. Numerical calculations are in agreement with the full-wave simulations as well as the antenna measurements which demonstrate functionality. The miniaturized and low cost antenna unit can be useful for space communications and other surveillance applications as well as network formations of small satellites where broad beam patterns with low gain values are required for adequate coverage.**

I. Introduction

The design, construction, testing, and launching of satellites is a very expensive process. However, satellites can be very effective and they are often the only viable method to achieve tasks in space from a remote location [1]-[3]. A possible solution for such space and communication applications is the use of microsatellites. When compared to conventional single satellite systems, microsatellite configurations can include a network of small satellites that can offer reduced launching costs and mission development time. These microsatellites and the even smaller nanosatellites and picosatellites, are becoming popular to perform specific space related research or geographical surveillance. They can also be relatively inexpensive when compared to more traditional satellite systems.

With such satellite miniaturization many new engineering challenges arise. One important aspect is antenna integration, as the satellite structure is often comparable, or even smaller, than the communications wavelength. Thus satellite size and weight restrictions inherently drive the need for innovative and compact feed systems and antennas with low cost. While the conventional half-wavelength microstrip patch may serve as a suitable antenna on conventional satellites using printed circuit board (PCB) technology at microwave frequencies, more compact implementations [4]-[9] may be needed for microsatellites.

Common techniques to reduce the physical size of printed microstrip antennas include the use of high dielectric constant materials [10], but narrowed bandwidth (BW) performances may be observed with these designs along with reduced radiation efficiencies. Other strategies for size reduction involve placing shorting pins near the probe feed, patch shape and feed optimization, slot inclusions, spur-line notching, and the very popular quarter-wave patch arrangement [11]-[14]. In [15], the quarter-wave concept was extended by proposing the idea of folding both the patch and the ground plane into two layers to create a folded-shorted patch. This procedure can further reduce the physical size of the quarter-wave patch.

Several preliminary investigations using this miniaturization technique have been reported [15]-[17] for a single metallic element offering linear polarization. In [18], the folded-shorted patch concept was recently implemented in an array configuration offering circular polarization (CP) at 400 MHz for operation on a microsatellite. This design also had a metallic construction and required very precise and expensive machining during its fabrication. Development of the folding technique into a planar antenna design that uses multilayer printed circuit board (PCB) manufacturing would enable low cost implementation. Such a microstrip-based structure was originally investigated in [19] by the assistance of commercial solvers. Similar radiation performances were obtained for the low cost PCB design to that of the earlier metallic implementation in [18]. A completely planar realization, as further developed and modeled in this paper, would allow for the addition of other performance improvement techniques that have been previously applied to printed antennas while also providing easier scaling to higher frequencies of operation.

We describe in this work the design and experimental verification of a new and highly integrated, low cost printed array of folded-shorted patches offering CP using standard PCB technology for use on microsatellites as well as other application where compact antenna structures are needed. Dimensions of the PCB antenna are 150 mm by 150 mm ($0.2\lambda_0$ by $0.2\lambda_0$) and measured gain values are greater than 0.4 dBic at about 400 MHz. Specific microsatellite applications of the four-layer design include low data rate communications in the UHF band for telemetry and remote sensing. In Section II of this paper an analysis of a single element is presented along with a simple but accurate transmission line model and tuning approach for antenna synthesis. Calculated resonant frequencies are in agreement with the full-wave simulations

S.K. Podilchak is with the Institute of Sensors, Signals, and Systems, School of Engineering and Physical Sciences, Edinburgh Campus, Heriot-Watt University, Edinburgh EH14 4AS, Scotland, UK. (e-mail: skp@ieee.org)

A.P. Murdoch is The Design Team Leader for Aerospace and Telecommunications Engineering Support Squadron (ATESS), within The Canadian Armed Forces, (e-mail: paul.murdoch@forces.gc.ca).

S.K. Podilchak and Y.M.M. Antar are with the Department of Electrical and Computer Engineering, Faculty of Engineering, The Royal Military College of Canada, Kingston, Ontario (e-mail: antar-y@rmc.ca).

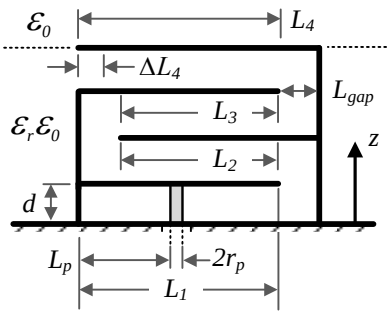

Fig. 1. Cross-sectional view of a four-layer folded-shorted patch implemented using PCB technology. The top of the ground plane is defined as the x-y plane with the z-axis oriented to the direction of the top air-dielectric interface.

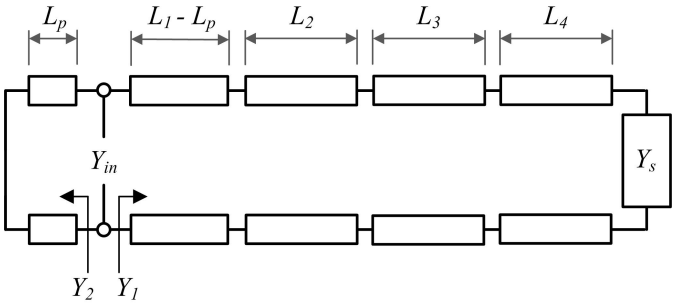

Fig. 2. Transmission line model for the four-layer ($N = 4$) folded-shorted patch. Segments L_1, L_2, L_3, and L_4 can be modeled by transmission lines (defined by W/d) where Y_s is the equivalent admittance for the radiating slot, Y_{in} is the input admittance at the feed point, and Y_1 and Y_2 are the input admittances looking into the shorting wall and slot, respectively.

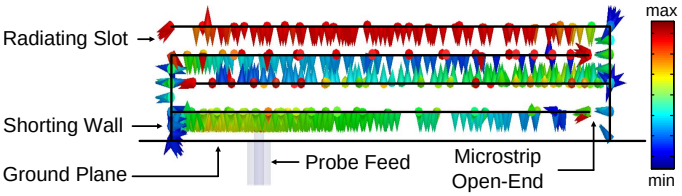

Fig. 3. Simulated electric field (in V/m) within the four-layer folded-shorted patch antenna at resonance. In particular, the electric field vector within the antenna structure is described by arrows with color defining magnitude or field strength (red defines a field maximum while blue defines a field minimum). The direction of the arrow represents phase. Fringing fields can be observed at the open edges of the four metallic layers (near the shorting wall and extended ground plane) and are defined by electric field maximums.

and our proposed transmission line model is also extended to an N-layer folded-shorted patch. Section III provides assembly details of the PCB, four-layer antenna and its measurement. To the best of our knowledge such a low cost, microstrip-based antenna, which is well suited for microsatellites, has not been investigated previously, which offers simple fabrication, good integration and a very compact size.

II. Principle of Operation and Antenna Modeling

The geometry of the folded-short patch (see Fig. 1) maintains the electrical length of the quarter-wavelength patch, however, the folding technique forces the fields to follow a meandered path enabling size reduction [16]-[18]. For example, the ground plane and shorted patch can be folded three times to achieve a compact folded-shorted patch with four layers having an electrical length of approximately a quarter-wavelength, but with a reduced physical antenna length of L_{max}. This total antenna length is related to the number of stacked layers; i.e. $L_{max} \approx \lambda_g/4N$ where λ_g is the guided wavelength and $N \geq 2$. In our case $\lambda_g = \lambda_0/\sqrt{\epsilon_r}$ and $N = 4$ since the antenna is four layers and implemented using a host dielectric substrate defined by ϵ_r as shown in Fig. 1.

A. Modeling of the Folded-Shorted Patch

To accurately predict the operation of the four-layer folded-shorted patch we advance the equivalent transmission line model which was originally presented in [15] and [16]. In particular, to improve model accuracy we include the physical effects of open-ended transmission line sections within the antenna structure and accommodate for its resulting modification to the effective patch length. We also do not make the assumption, as in [15], that all patch segments are of equal length within the four-layer antenna due to the folding and extending of the patch sections and ground plane; ie. $L_1 = L_4 \neq L_2 = L_3$ as shown in Fig. 2. This is because a small gap, newly defined in this work as L_{gap}, exists between the patch layers and the shorting wall.

Modeling techniques also include a simple tuning procedure which can assist in antenna performance optimization at the desired frequency of operation. Mainly, the radiating length of the top patch layer, L_4 (or transmission line section), can be altered by ΔL_4 as illustrated in Fig. 1. To the authors' knowledge this is the first time that such a detailed transmission line representation has been presented which also accurately models the fringing fields at the microstrip open edges.

In the next few sections we discuss the electric field distribution generated within the single element due to a probe excitation (Fig. 3). Then our proposed transmission line model is detailed and numerical calculations are compared in Fig. 4. Predicted resonant frequency values show agreement with the full-wave simulations. Simulated and calculated resonant frequency values as a result of element tuning are also compared in Fig. 5.

B. Electric Field within the Compact Antenna Structure

Electric field distributions are illustrated in Fig. 3 for the four-layer, folded-shorted patch antenna at resonance. Within the interior of the structure it can be observed that the electric field maximums are concentrated near the open edges of the four patch layers illustrating the fringing fields. Physically, a single radiating slot can be thought to form between the top two layers. Thus the far-fields originate from the current distributions generated near this radiating slot.

C. Transmission Line Modeling & Tuning Analysis

Following [6], [15]-[17] the input impedance, Z_{in}, at the probe feed can be defined by the complex load of the single element, Z_{ant}, and the probe reactance, X_p, mainly

$$\mathrm{Z}_{in} = Z_{ant} + jX_p\,, \quad \text{where}$$

$$\mathrm{X}_p = \frac{\omega\mu_0 d}{2\pi}\left[\ln\left(\frac{2}{kr_p}\right) - 0.57721\right], \quad \text{and}$$

$$\mathrm{Z}_{ant} = \frac{1}{Y_1 + Y_2}$$

$$= Z_0 \Bigg/ \left(\frac{Y_s + jY_0\tan\left(k_0\left(L - L_p\right)\right)}{Y_0 + jY_s\tan\left(k\left(L - L_p\right)\right)} + \frac{1}{j\tan\left(kL_p\right)}\right) \quad (1)$$

where $Z_0 (= 1/Y_0)$ is the characteristic impedance of the individual transmission line layers, $k = \omega\sqrt{\mu_0\epsilon_0\epsilon_r}$, L is the effective length of all the transmission line segments, and Y_s is the equivalent admittance defined by the slot conductance 'G_s' and susceptance 'B_s' for the radiating edge [6].

For improved accuracy in the prediction of the resonant length of the folded-shorted patch, we include the factor Δl_{oc} [20] to account for the fringing fields[1] near the open microstrip transmission lines. Specifically, to account for open-end effects within the folded antenna structure, we define the patch length 'L' of the combined transmission line layers as

$$L = L_1 + L_2 + L_3 + L_4 + 3\Delta l_{oc}\,. \quad (2)$$

The factor $3\Delta l_{oc}$ is included in Eq. (2) to provide an accurate prediction of the effective patch length and its relation to the physical patch length (defined here as $L_{max} = L_4 + L_{gap}$).

By following this approach the three open-ended sections for the lossless microstrip line can be further identified in Figs. 1 and 3 as follows: the junction between the metallic transmission line segments L_1 and L_2 (near the bottom of the right sidewall), near metallic segments L_2 and L_3 (in the middle of the antenna structure near the left sidewall), and at the junction of L_3 and L_4 (near the top of the right sidewall). The capacitive effective of the fourth open-ended microstrip line, due to the radiating slot and the corresponding effective length adjustment of the top transmission line section, is accounted for in the B_s suspetance term.

D. Numerical Results & Discussions

Figure 4 compares the calculated resonant frequency with and without the fringing field term (Δl_{oc}). In fact, if edge effects are not included in the antenna modeling, prediction errors in the resonant frequency can increase to beyond 10 MHz, in particular for this layer separation and W/d ratio where W and d are the width of the patch and its layer thickness, respectively. The resonant length of the folded-shorted patches can also be tunned by adjusting the top transmission line section by ΔL_4. This small modification can alter the radiating length of the folded-shorted patch and hence its resonant frequency. In practice this may be achieved by reducing the length of the top layer of the patch. Calculated resonant frequencies as a result of tuning are compared to simulations in Fig. 5 for the host dielectric (which was taken as free space, $\varepsilon_r = 1$) and values are in agreement. Hence,

[1]The equation for Δl_{oc} is not only useful for predicting the edge susceptance for a radiating slot, but is also an empirical formula (based on hybrid-mode full-wave analysis) to quantify the additional line length of an open-ended microstrip line [20].

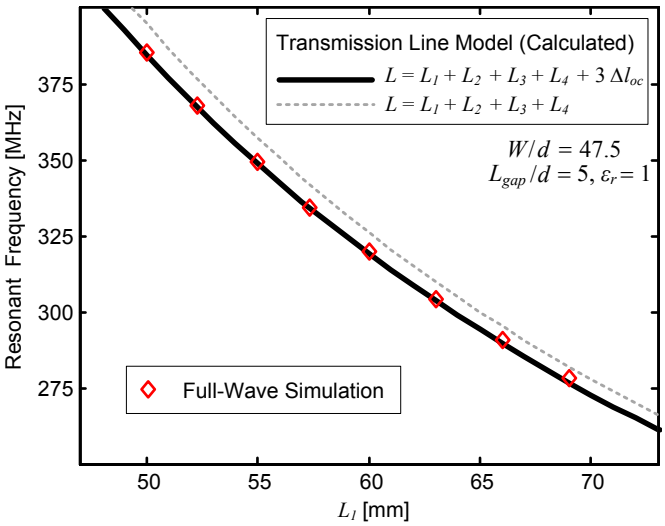

Fig. 4. Comparison of the calculated resonant frequency versus L_1 for the four-layer, folded-shorted patch with and without fringing field considerations.

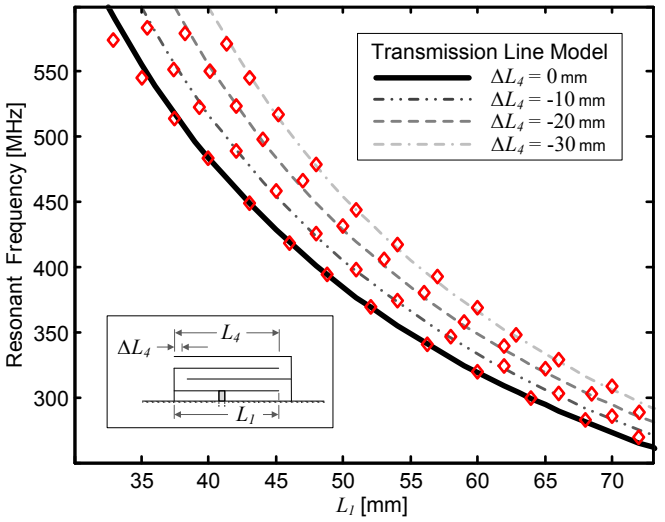

Fig. 5. Analysis of the tunable resonant frequency versus L_1 by altering the top vein length by ΔL_4. Full-wave simulations (red ◇) are in agreement with the calculations (black/grey dash-dot lines) using the proposed transmission line model for the four-layer folded-shorted patch ($W/d = 47.5$ and $L = L_1 + L_2 + L_3 + L_4 + 3\Delta l_{oc} + \Delta L_4$).

the resonant frequency of the patch elements can be tuned to accommodate for the results of fabrication and any variations of the dielectric constant from rated values. Thus, by reducing the length of the top layer, gain and reflection loss values can be optimized for the antenna system.

It should also be noted that the proposed transmission line model is accurate when d_{max} is much smaller than L_{max} (by at least 5 times [15]) and this explains the reduced accuracy when predicting the resonant frequency for $L_1 \leq 37$ mm in Fig. 5. In addition, for $L_1 > 70$ mm minor differences between the full-wave simulations and calculations can be observed due to the increased layer size with respect to the wavelength. Regardless, general agreement is still observed and this suggests that the presented transmission line model is suitable for patch layer lengths that are greater than 5% of

the wavelength.

Improvements in the model are also possible by including the reactive effects within the antenna structure due to the separation between the shorting wall and the metallic layers (L_{gap}), the added inductance due to the shorting wall, and the extended ground plane. Nevertheless, calculations are in agreement with the full-wave simulations. Thus, the proposed transmission line model and extension to single element tuning, may be useful for the design of such folded-shorted patches.

E. Model for an N-layer Folded-Shorted Patch

The proposed transmission line model for the four-layer folded-shorted patch outlined in the last few sections can be generalized to an N-layer design. First we modify Eq. (2), the effective electrical length of the antenna 'L', to account for the possibility of 'N' different layers:

$$L = L_1 + L_2 + \cdots + L_{N-1} + L_N + (N-1)\,\Delta l_{oc}\,, \qquad (3)$$

where $N \geq 2$. In addition, the physical antenna length 'L_{max}' can be related to the resonant frequency, f_r:

$$L_{max} \approx \frac{c}{4N f_r} + N\,\Delta l_{oc}\,, \qquad (4)$$

where c is the phase velocity in vacuum and

$$f_r \approx \frac{c}{4\,(L_1 + L_2 + \cdots + L_{N-1} + L_N + N\,\Delta l_{oc})}\,. \qquad (5)$$

Calculations of the input impedance and the exact resonant frequency (defined in this paper as $\Im\mathrm{m}\{Z_{in}\} = 0$) can also be completed for an N-layer folded shorted patch using Eqs. (1) and (3). Moreover, the impedance BW can also be related to the number of N-layers since it has been observed in [16] and [18], that bandwidth decreases for an increase in N but also broadened by enlarging the air gap separation 'd' between layers:

$$\mathrm{BW} \propto \frac{d}{N}\,. \qquad (6)$$

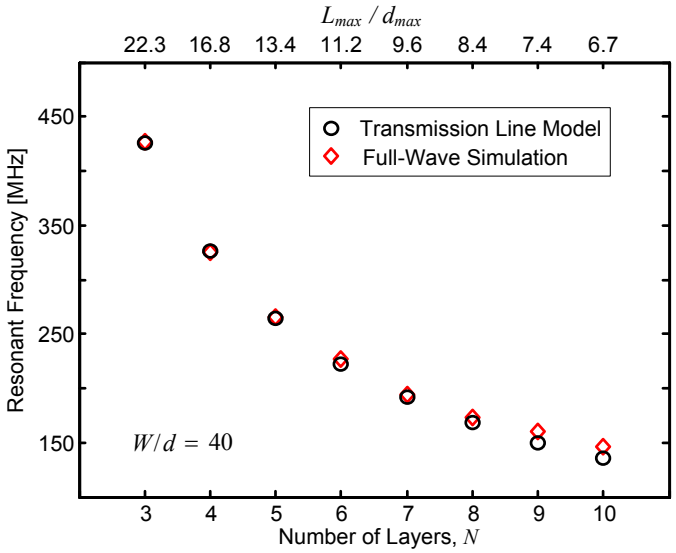

Fig. 6. Calculated and simulated resonant frequencies for an N-layer folded-shorted patch element (all structures defined with L_{max} = 67 mm). Here d_{max} is defined as the total height of the folded-shorted patch.

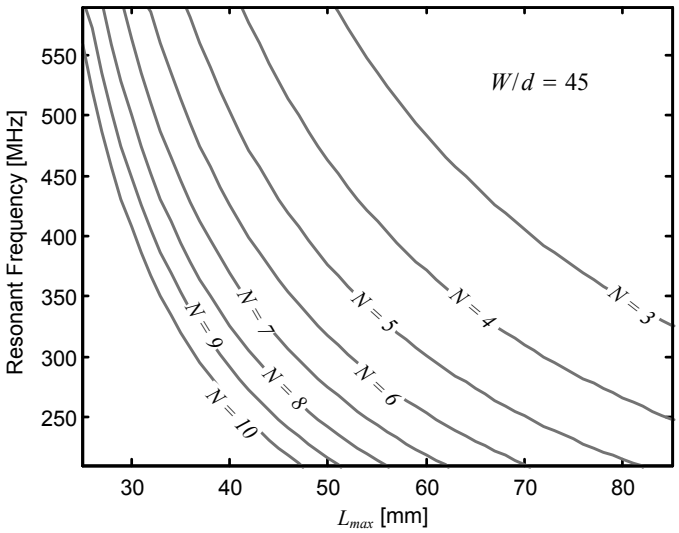

Fig. 7. Resonant frequency versus L_{max} (N defines the number of layers).

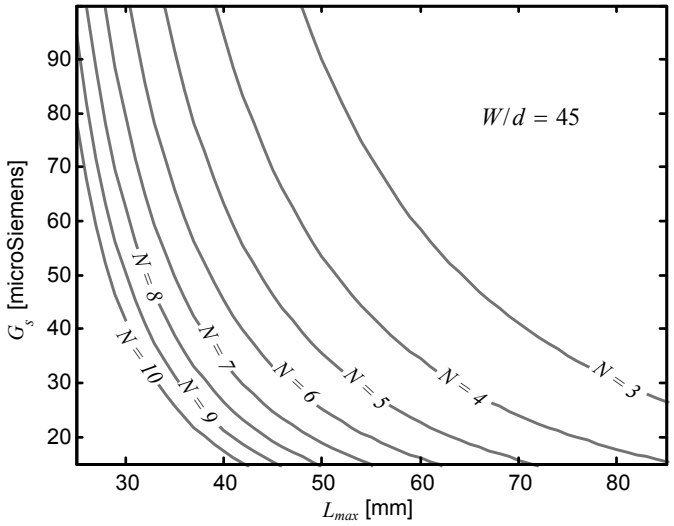

Fig. 8. Radiation conductance G_s calculated at resonance versus L_{max}.

Calculated resonant frequency values are shown in Fig. 6 up to and including a ten-layer folded-shorted patch. Results are in agreement with the full-wave simulations. As discussed in the previous sections, the proposed transmission line model is accurate when d_{max} is much smaller than L_{max} and thus explains the reduced accuracy for the predicted resonant frequencies when $N \geq 8$. The resonant frequency is also plotted versus L_{max} in Fig. 7 and the corresponding slot conductance (Fig. 8) at patch resonance. It can be observed that for L_{max} = 50 mm, the resonant frequency for the folded-shorted patch can vary by about 40% (from 600 MHz to 240 MHz) for $N = 3$ to $N = 8$. Moreover, the corresponding slot conductance is reduced by approximately 25% for the $N = 8$ design when compared to the three-layer configuration

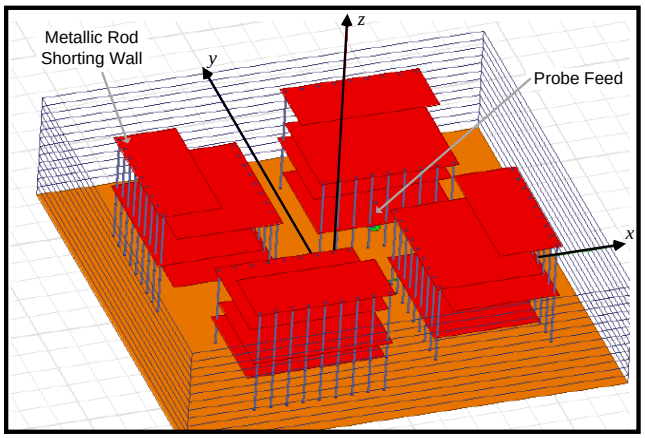

Fig. 9. Designed HFSS model of the array for CP with the ground plane and the folded-short patches shown in orange and red, respectively. The x, y, z coordinate system is defined at the centre of the structure and directly above the ground plane.

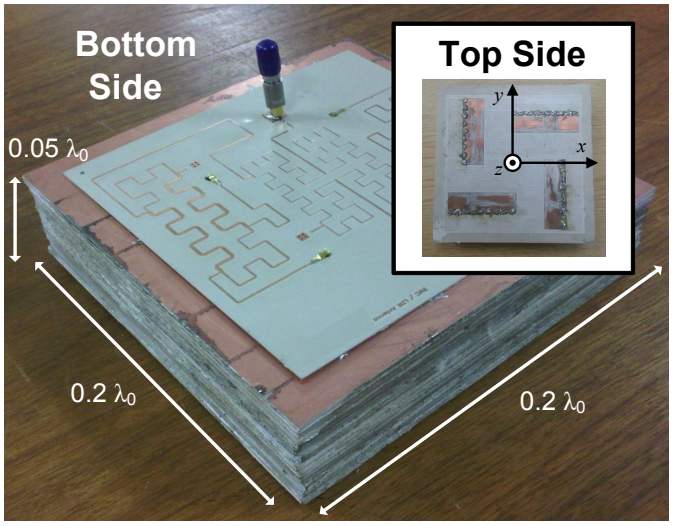

Fig. 10. The fabricated and measured multilayer PCB prototype with the integrated feeding circuit.

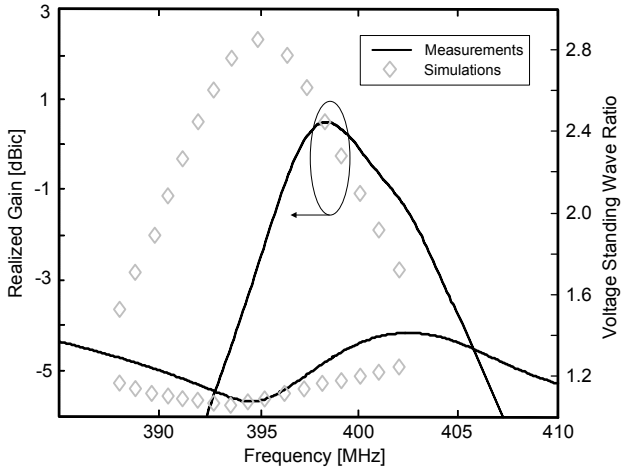

Fig. 11. Comparison between the measured and simulated realized gain and VSWR (50-Ω impedance). Measured values recorded using a calibrated far-field anechoic chamber.

($N = 3$). This signifyies a reduced radiated power with an increase in the number of layers. Figures 6, 7, and 8 can be useful for the antenna engineer to recognize the relative amount of radiated power when compared to the number of N-layers, physical patch size, and the resulting resonant frequency when designing compact and planar foled-shorted patches for microsatellite.

III. Antenna Design, Results, & Discussion

One method of producing CP is to arrange four linearly polarized elements (sequentially rotated) and with a 90° offset in phase [18], [22]. Utilizing the feeding circuit as previously outlined by the authors in [18], a new multilayer PCB implementation of the antenna structure was designed and simulated using HFSS [21] for operation at 395 MHz (see Fig. 9). The multilayer structure was then created by wet etching techniques (in house) at The Royal Military College of Canada. The shorting walls were implemented by metallic rods of appropriate length which were soldered and drilled through the PCB layers. Also, the substrate material Rogers 6002™ was chosen for its relatively low dielectric constant and loss tangent, 2.94 and 0.0012, respectively. Twelve substrate panels were stacked to make the four layers of the patches and this assembly was completed using an adhesive spray. The size of the miniaturized and ultra compact antenna with the integrated feed system was 150 mm by 150 mm by 37 mm ($0.2\lambda_0$ by $0.2\lambda_0$ by $0.05\lambda_0$) while the individual patches were 30 mm in width and 39 mm in length with a height 36.6 mm. See Fig. 10 for a photograph of the fabricated antenna structure.

Simulation results show that maximum gain values of 2.3 dBic (RHCP) can be obtained at 395 MHz which are similar to the metallic implementation in [18]. Comparison of the simulated and measured antenna gain, parametric sweeps of important dimensions, and the matching versus frequency are shown in Figs. 11 and 12 for the PCB design as well as the beam pattern in Fig. 13 at the observed measured maximum of 397.5 MHz. These plots show that the measured antenna matching, the CP gain, and the beam pattern (co-polarized, RHCP) are in general agreement with the simulations.

Parametric sweeps were completed to further simulate and investigate the effects of the fabrication and assembly on the realized gain of the antenna. Results are reported in Fig. 12. One parameter was investigated while others were held constant. This is important to explain any discrepancies between the measurements and that of the optimized and simulated structure for operation at 395 MHz. As shown in Fig. 12, if the probe position for a single radiating element is altered from the optimal position by up to 1.5 mm, there is a slight change in the total realized gain for the structure (less than 0.5 dB) as well as a minor upward shift in the operation frequency. Now with a horizontal positioning of the top dielectric layer by 1 mm in the x- and y-directions, the realized gain can decrease by about 1 dB. It is also interesting to note that similar effects can still be observed with a shift of only 0.25 mm. However, if an air gap is included between all twelve of the dielectric layers which define the total antenna

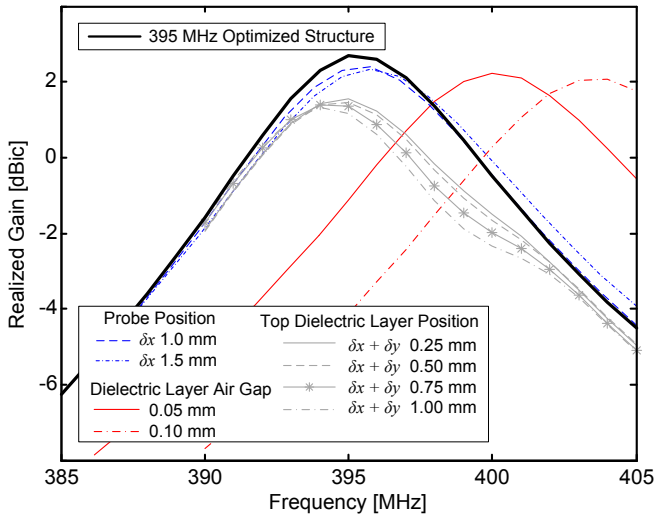

Fig. 12. Effect of the practical fabrication tolerances on the realized antenna gain: probe position variation along the x-direction for the radiating element in the first quadrant, an air-gap between all twelve dielectric layers of the structure, and a horizontal shift for the top dielectric layer (only) along the x- and y-directions. Results are also compared to the realized gain simulations from Fig. 11.

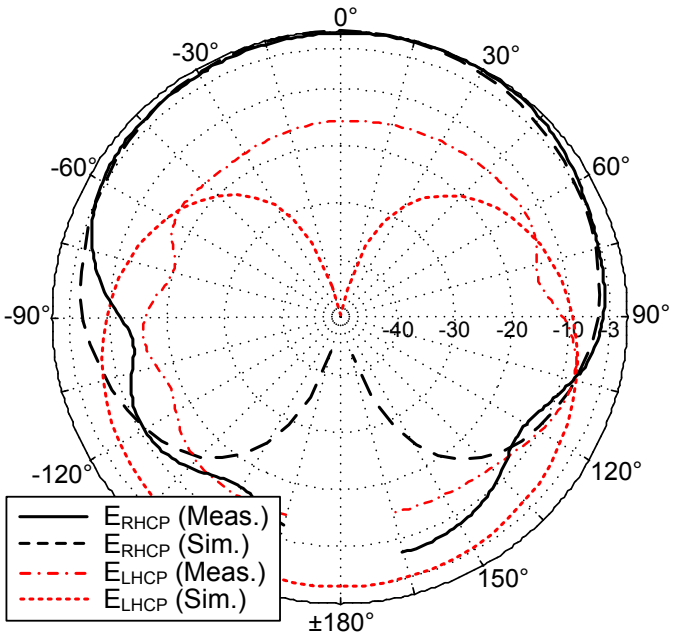

Fig. 13. Normalized beam patterns in the $\phi = 0°$ plane for the PCB antenna.

structure, a frequency shift can still be observed along with a minor degradation in the maximum realized antenna gain. For example, with a 0.05 mm air gap, the maximum realized gain is still above 2 dBic but at 400 MHz. For the fabricated and measured antenna structure it was likely that a minor air gap between the dielectric layers was present (<0.05 mm) which shifted the frequency for the maximum realized gain to 397.5 MHz, as well as a minor misalignment for one of the dielectric layers which reduced the measured gain to about 0.6 dBic as shown in Fig. 11.

The cross polarization levels for the fabricated antenna are higher than the simulated values where a null at broadside

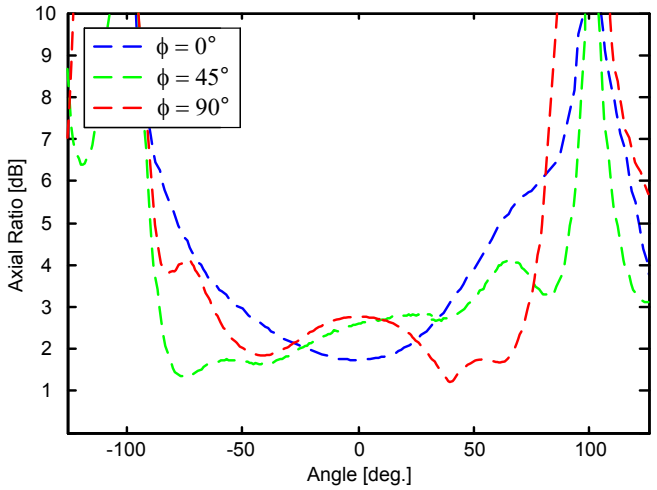

Fig. 14. Measured axial ratio versus angle at 398 MHz.

can be observed. Also, the quality of the polarization in terms of the measured axial ratio versus beam angle for each plane is plotted in Fig. 14; similar values were reported in [18]. Deviations between the measurements and the simulations for the cross-polarization levels in this work may be attributed to the above mentioned practical fabrication and assembly tolerances, variations in the dielectric constant of the utilized feeding circuit, cable bending and twisting during the antenna measurements, and the possible interference of the antenna positioner and the measurement cable attached to the SMA connector of the antenna prototype.

It should be mentioned that the high-cross pol. radiation (LHCP) into the antenna backside, as shown in Fig. 13, is not much of a concern for our compact microsatellite antenna, mainly since the main co-pol. pattern (RHCP) can be aligned with that of the base station antenna with cross-pol. radiation into vacant space. This is made possible by appropriate placement on the satellite structure. Regardless of the minor discrepancies with that of the simulations and measurements, general agreement can still be observed. As described, the deviations between the simulated and measured designs can be attributed to fabrication and assembly tolerances, air gaps between the dielectric layers, minor probe misalignment, and practical difficulties in measuring such a miniaturized CP antenna.

IV. Conclusion

This work has described the design, simulation, and measurement of a folded-shorted patch array offering circular polarization. An accurate but simple transmission line model for the antenna was developed by including the effects of open-ended microstrip transmission lines within the structure. Numerical calculations are in good agreement with the full-wave simulations. Using this theoretical model as a starting point, HFSS simulations were carried out to optimize functionality. Experimental performance of a prototype implemented using PCB technology was then measured and analyzed. Results support the design procedure using the proposed transmission

line modeling as well as the simulation findings. The demonstrated circularly polarized folded-shorted patch antenna, using multilayer PCB technology, is a good candidate for UHF telemetry communications for microsatellite applications, in particular, where antenna cost and antenna size are important.

REFERENCES

[1] J.K. Kreng, M.M. Ardeshiri, O.C. Barbosa, and Y.Y. Krikorian, "Telemetry, Tracking, and Commanding (TT&C) Link Considerations for a LEO Sat," *2005 IEEE Aerospace Conf.*, pp. 1646–1655, Mar. 2005.

[2] S. Gao, K. Clark, A. Sharaiha, M. Unwin, J. Zackrisson, W.A. Shiroma, J.M. Akagi, K. Maynard, P. Garner, L. Boccia, G. Amendola, G. Massa, C. Underwood, M. Brenchley, M. Pointer, and M.N. Sweeting, "Antennas for Modern Small Satellites," *IEEE Antennas and Propagation Magazine*, vol. 51, no. 4, pp. 40-56, Aug. 2009.

[3] L. Jianzhou, Q. Chen, Y. Zhang, and C. Wu, "Design of TTC antenna for mini-satellite application," *2011 IEEE Signal Processing, Communications and Computing Conf.*, pp. 1–3, Sep. 2011.

[4] K. Fujimoto, A. Henderson, K. Hirasawa, and J.R. James, "Small Antennas," London, U.K.: Research Studies Press, 1987.

[5] J.R. James and P.S. Hall, "Handbook of Microstrip Antennas," Peter Peregrinus Ltd., London, U.K., 1989.

[6] R. Garg, P. Bhartia, I. Bahl, A. Ittipiboon, "Microstrip antenna design handbook," Artech House Publishers, Norwood, MA, USA 2001.

[7] K.L. Wong, "Compact and Broadband Microstrip Antennas," John Wiley & Sons, Inc., New York, NY, USA 2002.

[8] R. B. Waterhouse, S. D. Targonski, and D. M. Kokotoff, "Design and Performance of Small Printed Antennas," *IEEE Trans. Ant. Prop.*, vol. 46, no. 11, pp. 1629-1633, Nov. 1998.

[9] A.K. Skrivervik, J.F. Zurcher, O. Staub, and J.R. Mosig, "PCS antenna design: the challenge of miniaturization," *IEEE Antennas and Propagation Magazine*, vol. 43, no. 4, pp. 12-27, Aug. 2001.

[10] T. K. Lo, C.-O. Ho, Y. Hwang, E. K. W. Lam, and B. Lee, "Miniature Aperture-Coupled Microstrip Antenna of Very High Permittivity," *IET Electronics Letters*, vol. 33, no. 1, pp. 9-10, Jan. 1997.

[11] S. Pinhas and S. Shtrikman, "Comparison Between Computed and Measured Bandwidth of Quarter-Wave Microstrip Radiators," *IEEE Trans. Ant. Prop.*, vol. 36, no. 11, pp. 1615-1616, Nov. 1988.

[12] M. Sanad, "Effect of the shorting posts on short circuit microstrip antennas," *Proc. IEEE Antennas and Propagation Society International Symposium*, vol. 2, pp. 794–797, Jun. 1994.

[13] K.L. Wong and K.P. Yang, "Modified planar inverted F antenna," *IET Electronics Letters*, vol. 34, no. 1, pp. 7-8, Jan. 1998.

[14] W.S. Chen, K.L. Wong, and C.K. Wu, "Inset microstripline-fed circularly polarized microstrip antennas," *IEEE Trans. Ant. Prop.*, vol. 48, no. 8, pp. 1253-1254, Aug. 2004.

[15] R. Li, G. DeJean, M. M. Tentzeris, and J. Laskar, "Development and Analysis of a Folded Shorted-Patch Antenna With Reduced Size," *IEEE Trans. Ant. Prop.*, vol. 52, no. 2, pp. 555–562, Feb. 2004.

[16] J. Zhang and O. Breinbjerg, "Miniaturization of Multiple-Layer Folded Patch Antennas," *European Conference on Antennas and Propagation*, pp. 3502–3506, 23-27 Mar. 2009.

[17] A. Holub and M. Polivka, "Vertically Meander-Folded, Shorted-Patch Antennas," *Wiley Microwave and Optical Tech. Lett.*, vol. 51, no. 12, pp. 2938–2942, Dec. 2009.

[18] S.K. Podilchak, M. Caillet, D. Lee, Y.M.M. Antar, L. Chu, M. Hammar, D. Caldwell, and E. Barron, "A Compact Circularly Polarized Antenna using an Array of Folded-Shorted Patches," *IEEE Transactions on Antennas and Propagation*, vol. 61, no. 9, pp. 4861-4867, Sept. 2013.

[19] A.P. Murdoch, S.K. Podilchak, and Y.M.M. Antar, "A Compact Circularly Polarized Multilayer Printed Antenna for Use on Micro-Satellites," *IEEE AP-S*, Chicago, USA, 2012.

[20] M.R. Kirschning, R.H. Jansen, and N.H.L. Koster, "Accurate Model for Open End Effect of Microstrip Lines," *Electron. Lett.*, vol. 17, pp. 123–125, 1981.

[21] "High Frequency Structure Simulator v. 12.0," Ansoft Corp, 2012 [Online]. Available: www.ansys.com

[22] J. Huang,"A Technique for an Array to Generate Circular Polarization with Linearly Polarized Elements," *IEEE Trans. Ant. Prop.*, vol. 34, no. 9, pp. 1113-1124, Sep. 1986.

Symon K. Podilchak (S'03–M'05) received the B.A.Sc. degree in Engineering Science from the University of Toronto, ON, Canada, in 2005, and the M.A.Sc. degree in Electrical Engineering from The Royal Military College of Canada, Kingston, ON, in 2008. In 2013 he received the Ph.D. degree in Electrical Engineering from Queen's University, Kingston, ON, which was awarded an Outstanding Dissertation Award from the same university.

He joined the Department of Electrical and Computer Engineering at Queen's University in Kingston, Ontario, Canada as a Lecturer in 2010 where he contributed to the development and teaching of electromagnetics, electronics, and design-based courses at the graduate and undergraduate level. During this same period, he has also been a Research Associate at The Royal Military College of Canada. In 2013 he became an Assistant Professor at Queen's, and in 2015 he joined the Institute of Sensors, Signals, and Systems at Heriot-Watt University, Edinburgh, United Kingdom.

Dr. Podilchak has also had experience as a computer programmer and assisted in the design of radomes for 77 GHz automotive radar. Recent industry experience also includes the modeling and design of high frequency surface-wave radar and noise radar systems, and professional software design and implementation for antenna measurements in anechoic chambers as well as control of the SLOWPOKE Nuclear Reactor Facility in Kingston, ON, Canada for The Department of National Defence. Dr. Podilchak has also designed compact multiple-input multiple-output (MIMO) antennas for wideband military communications as well as highly compact circularly polarized antennas for microsatellites. His research interests include surface waves, leaky-wave antennas, metasurfaces, UWB antennas, retrodirective arrays, wireless power transmission, and CMOS integrated circuits.

Dr. Podilchak is a registered Professional Engineer (P.Eng.) in the Province of Ontario. He has been the recipient of many best paper awards and scholarships; most notably Research Fellowships from the IEEE Antennas and Propagation Society, as well as, the IEEE Microwave Theory and Techniques Society. He has also been awarded a Fellowship from the Natural Sciences and Engineering Research Council of Canada (NSERC), a Horizon 2020 Marie Skłodowska-Curie European Research Fellowship, and four Young Scientist Awards from the International Union of Radio Science (URSI). In 2011 and 2013 he received student paper awards at the IEEE International Symposium on Antennas and Propagation, and in 2012, the best paper prize for Antenna Design at the European Conference on Antennas and Propagation. In 2014, the IEEE Antennas and Propagation Society recognized Dr. Podilchak as an Outstanding Reviewer for the IEEE Transactions on Antennas and Propagation, and in 2016, he received the Microwave Prize at the European Microwave Week for his PhD research work. Dr. Podilchak is also the founding chairman of the IEEE Antennas and Propagation Society and the IEEE Microwave Theory and Techniques Society, Joint Chapter of the IEEE Kingston Section. In recognition of these services, the IEEE presented Dr. Podilchak with an Outstanding Volunteer Award. Currently he serves as Associate Editor for IET Electronic Letters.

Captain Paul Murdoch CD, BEng, MASc. Canadian Armed Forces (CAF). MASc Electrical Engineering, RMCC, 2012. Currently Senior Design Engineer at the RCAF Engineering Support Squadron, where he is responsible for avionics integration and installation designs.

Yahia M. M. Antar (S'73–M'76–SM'85–F'00–LF'13) received the B.Sc. (Hons.) degree in 1966 from Alexandria University, Alexandria, Egypt, and the M.Sc. and Ph.D. degrees from the University of Manitoba, MB, Canada, in 1971 and 1975, respectively, all in electrical engineering. In 1977, he held a Government of Canada Visiting Fellowship at the Communications Research Centre in Ottawa, ON, where he worked with the Space Technology Directorate on communications antennas for satellite systems. In May 1979, he joined the Division of Electrical Engineering, National Research Council of Canada, Ottawa, where he worked on polarization radar applications in remote sensing of precipitation, radio wave propagation, electromagnetic scattering, and radar cross-section investigations. In November 1987, he joined the staff of the Department of Electrical and Computer Engineering, Royal Military College of Canada, Kingston, ON, where he has held the position of professor since 1990 and is presently Vice Dean for defence and security research. He has authored or coauthored close to 200 journal papers, many chapters in books, about 400 refereed conference papers, holds several patents, has chaired several national and international conferences, and has given plenary talks at many conferences. He has supervised and co-supervised over 80 Ph.D. and M.Sc. theses at the Royal Military College and at Queen's University, of which several have received the Governor General of Canada Gold Medal, the outstanding Ph.D. Dissertation Award, as well as many best paper awards in major international symposia. He served as the Chairman of the Canadian National Commission for Radio Science (CNC, URSI, 1999-2008), Commission B National Chair (1993-1999), held adjunct appointment at the University of Manitoba, and has a cross appointment at Queen's University in Kingston.

Dr. Antar is a Life Fellow of the IEEE (Institute of Electrical and Electronic Engineers), a Fellow of the Engineering Institute of Canada (FEIC), a Fellow of the Electromagnetic Academy, serves as an Associate Editor of the IEEE Antennas and Propagation Magazine, served as Associate Editor of the IEEE Transactions on Antennas and Propagation, the IEEE Antennas and Wireless Propagation Letters, IET, and was a member of the Editorial Board of the RFMiCAE Journal. He served on NSERC grants selection and strategic grants committees, Ontario Early Research Awards (ERA) panels, and on review panels for the National Science Foundation in the U.S. In May 2002, he was awarded a Tier 1 Canada Research Chair in Electromagnetic Engineering which has been renewed in 2016. In 2003, he was awarded the Royal Military College of Canada "Excellence in Research" Prize, and the RMCC Class of 1965 Teaching Excellence award in 2012. He was elected by the Council of the International Union of Radio Science (URSI) to the Board as Vice President in August 2008 and in 2014, and to the IEEE Antennas and Propagation Society Administration Committee in December 2009. On January 31, 2011, he was appointed Member of the Canadian Defence Science Advisory Board (DSAB). He served as an IEEE Antennas and Propagation Society Distinguished Lecturer. In October 2012, he received the Queen's Diamond Jubilee Medal from the Governor General of Canada in recognition for his contribution to Canada. He is the recipient of two national awards: the 2014 IEEE Canada RA Fessenden Silver Medal, and the 2015 IEEE Canada J. M. Ham outstanding Engineering Education Award. In May 2015, he received the RMC Cowan Prize for excellence in research.